

# Young massive stars and their environment in the mid-infrared at high angular resolution

W.J. de Wit<sup>1</sup>, M.G. Hoare<sup>1</sup>, R.D. Oudmaijer<sup>1</sup>, T. Fujiyoshi<sup>2</sup>

<sup>1</sup> School of Physics & Astronomy, University of Leeds, LS2 9JT, UK

<sup>2</sup> Subaru Telescope, NAOJ, 650 North A'ohoku Place, Hilo, HI 96720, USA

E-mail: w.j.m.dewit@leeds.ac.uk

**Abstract.** We present interferometric and single-dish mid-infrared observations of a sample of massive young stellar objects (BN-type objects), using VLTI-MIDI ( $10\,\mu\text{m}$ ) and Subaru-COMICS ( $24.5\,\mu\text{m}$ ). We discuss the regions S140, Mon R2, M8E-IR, and W33A. The observations probe the inner regions of the dusty envelope at scales of 50 milli arcsecond and  $0.6''$  ( $\sim 100$ - $1000$  AU), respectively. Simultaneous model fits to spectral energy distributions and spatial data are achieved using self-consistent spherical envelope modelling. We conclude that those MYSO envelopes that are best described by a spherical geometry, the commensurate density distribution is a powerlaw with index  $-1.0$ . Such a powerlaw is predicted if the envelope is supported by turbulence on the  $100$ - $1000$  AU scales probed with MIDI and COMICS, but the rôle of rotation at these spatial scales need testing.

## 1. Introduction

Massive stars ( $> 8M_{\odot}$ ) play a major role in the dynamical, thermal and chemical evolution of galaxies. The question of how massive stars form is therefore central for a proper understanding of these processes. Currently there is no consensus regarding the answer to this question, and two diverging viewpoints regarding the initial formation stages are generally referred to. On the one hand, a high-mass star is formed from the monolithic gravitational collapse of a massive molecular condensation (core). The principal stellar product is a single or binary massive star that is formed from gravitationally bound core material [1] and accreted onto the central star through a disk. The competing viewpoint is due to [2] in which a massive core fragments into a collection of equal mass stellar seeds that compete via Bondi-Hoyle accretion for inflowing material. The seed that ends up being a massive star happened to be located in a fortuitous spatial position (near the centre of the potential well) where most of the inflowing material gathered. The amount of observational evidence [3–6] and theoretical considerations [7, 8] that favour the monolithic collapse scenario is growing. Recent developments in massive star formation are reviewed in [9, 10].

Whichever scenario dictates massive star formation (SF), they both start out with a massive and cold molecular core that is gravitationally unstable. Hidden from direct view by the surrounding dusty envelope, a massive star forms at the centre of the cold core and its radiation is reprocessed to longer wavelengths before it escapes the structure. Observations in the infrared (IR) and (sub)mm of star forming regions in the solar neighbourhood have identified cold objects with bolometric luminosities equalling that of a (single) massive star, i.e. a few times  $10^4 L_{\odot}$ . This luminosity is such that the central object has the ability to ionise its surroundings if due to

a single main sequence star, yet only little (if any) recombination emission is observed from these sources. These objects are identified with the massive young stellar object (MYSO) evolutionary phase of SF in which the formation of a central massive star is nearing its completion but the central object still experiences mass accretion. The latter is evidenced by the ubiquitous bipolar outflow signatures associated with these star forming regions [11]. The star itself, although unmistakably present, is not observable as the surrounding dusty envelope is highly optically thick ( $A_v$  up to 50 to 100). However crucial clues to the formation process can be conveyed by the radial structure of the dust envelope. It is determined by the forces that operate during the onset and the subsequent evolution of the initial molecular core. For example, the radial density profile is predicted to have a powerlaw with a value for the power index that depends on the dominant physics. The envelope emission is a direct consequence of the dust radial density distribution and the exact power index can be extracted from the observables by the use of radiative transfer models. Spherical envelope geometries can be assumed for the dust emission dominating at wavelengths larger than  $30\mu\text{m}$ , where the SEDs of MYSOs are observed to be remarkably similar, arguing for little deviation from spherical symmetry [12–21]. Emission of MYSOs at shorter wavelengths poses more serious interpretation problems.

Here we present an investigation into the structure of dusty MYSO envelopes at intermediate and high angular resolution in the mid-IR. We discuss Subaru-COMICS observations at  $24.5\mu\text{m}$  with an angular resolution of  $0.6''$  of a sample of 14 MYSOs, and VLTI-MIDI observation at  $10\mu\text{m}$  of 1 MYSO with a resolution of 50 milli arcseconds.

## 2. Observations and method of analysis

Observations at  $24.5\mu\text{m}$  were taken with the mid-infrared imaging spectrometer COMICS [22] mounted on the 8.2m Subaru telescope on Mauna Kea. The system attains a diffraction limited angular resolution of  $0.6''$  and delivers over-sampled images with  $0.13 \times 0.13 \text{ arcsec}^2$  pixels. A total of 14 well-known young massive stars were observed in a snapshot mode between 2003 and 2006. More details on observations and data reduction can be found in de Wit et al. (2008 subm.). The spatially resolved Subaru observations were used to construct an azimuthally averaged intensity profile as function of distance from the centre of the object.

The highest resolution observation presented here (50 mas) were taken with the MIDI instrument on the VLT interferometer. MIDI delivers spectro-interferometric information over the wavelength interval  $8\text{--}13\mu\text{m}$ . This set consists of 1 baseline on the MYSO W33A. The observations were taken using the UT2-UT3 telescope configuration for a projected baseline of 45.5m and position angle of  $47^\circ$  east of north; this is perpendicular to the star’s outflow direction. More details regarding observations and reduction can be found in [23]. The spatially resolved MIDI observations deliver the size scale of W33A as function of wavelength.

The analysis of the Subaru and MIDI data were quite analogous. Spatial information is combined with the SED, and we attempt to simultaneously model these observational data with spherical dust radiative transfer models. The spherical models were calculated with DUSTY, a code that solves the 1-D scaled radiative transfer problem [24]. SEDs were built from literature data. The Subaru sample was compared to a grid of 120 000 DUSTY models, whereas the best model for W33A was found iteratively.

We present the results regarding MYSO envelope emission going from the outside (Subaru) in (MIDI). First, we discuss the type of morphology observed in the resolved Subaru images.

## 3. The $24.5\mu\text{m}$ morphology of MYSOs

The COMICS images show that the main emission component at  $24.5\mu\text{m}$  is found in discrete single sources down to the angular resolution limit. These sources are invariably identified with the known MYSOs of each particular region. The majority of sources in our sample shows to first order symmetric  $24.5\mu\text{m}$  emission. In three cases the discrete sources are resolved

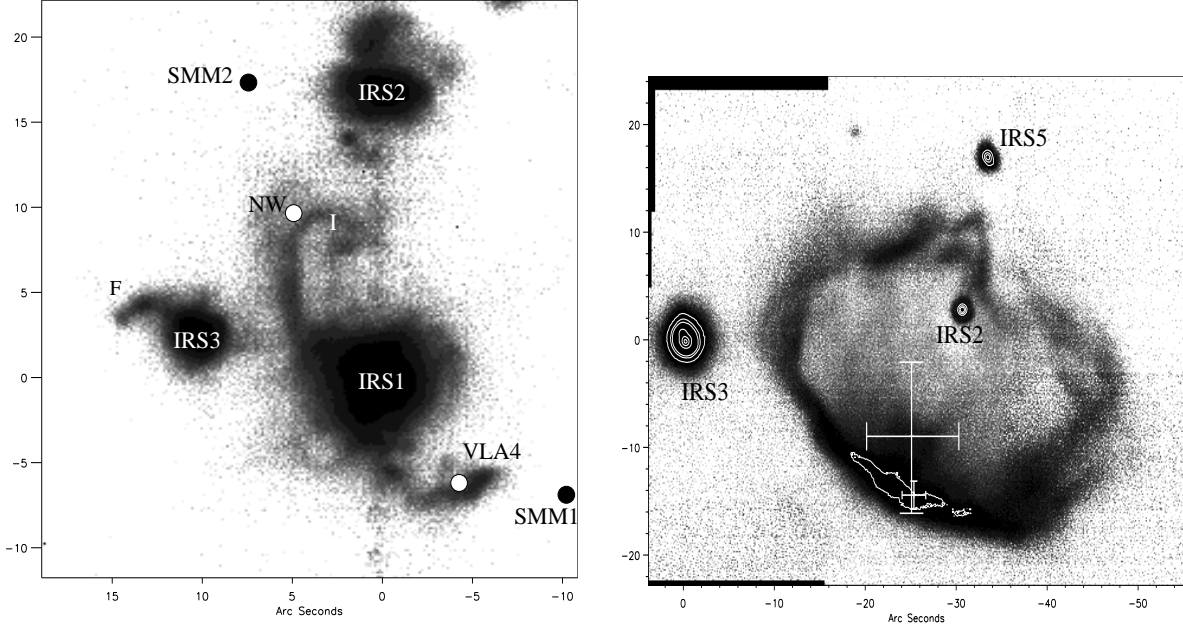


**Figure 1.** COMICS images at  $0.6''$  resolution of the S140 (left) and Mon R2 (right) massive star forming regions. Known sources and features have been annotated (see text). A vertical band of emission in the S140 image at abscissa  $\sim 0''$  is an image artefact.

in multiple condensations located within a resolved envelope (AFGL 961, AFGL 4029, W3). Extended diffuse emission is observed in many regions and is associated with either UCHII regions or with shock excited material. The systematic difference in morphology between UCHII and MYSOs demonstrates what is likely to be a difference in evolutionary phase: the break-out of ionised gas of the more evolved UCHII has lifted the dusty core remnant. The following subsections describe two examples of discrete and extended  $24.5\,\mu\text{m}$  emission as observed with COMICS.

### 3.1. The mid-IR morphology of the S140 region

At a distance 910 pc, the S140 massive star forming region is arguably the best example of the initial stages of massive star formation in the solar neighbourhood [25]. It consists of a cluster of at least three luminous near-IR sources without optical counterparts [26], and strong outflow activity. Detailed studies have demonstrated that the source IRS 1 consists of a disk found at a position angle of  $\sim 44^\circ$ , perpendicular to the CO outflow and monopolar reflection nebula [27, 28].

The left panel of Fig. 1 reveals a wealth of features associated with objects previously identified at different wavelengths. Discrete peaks in mid-IR emission are found at the positions of IRS 1, 2, and 3. IRS 1 is symmetric, whereas IRS 2 and IRS 3 are elongated. The latter is found to be a triple system [29] and our image partly resolves the secondary object (IRS3b) at a distance of  $0.75''$  east of the primary source (IRS3a).

The COMICS image also shows patches of diffuse emission that are found coincident with the radio sources VLA4 and NW [30]. This is the first time that the two radio sources are seen in the mid-IR. Previously [30], they were found coincident with the brightest parts of very extended near-IR nebosity. Noticeable is the spectacular arc of mid-IR emission labelled ‘I’. This dust emission structure concurs with an emission arc at  $K$ -band. The causes for the formation of this relatively large structures is unclear, as they do not align with the principal IRS1 outflow

direction. Finally, the curved wisp of mid-IR emission at  $\sim 3''$  from IRS3 corresponds to feature “F” of [29]. This feature demonstrates strongly polarised emission and strong  $\text{H}_2$  line emission. The structure is possibly created by outflow activity from IRS3. Perhaps surprisingly, we find no warm dust emission associated with the two submm emission peaks [31] that lie within our COMICS field. The S140 region shows  $24.5\mu\text{m}$  emission to have a diffuse character when it apparently traces shocked dense material, but also when it is associated with radio sources.

### 3.2. The mid-IR morphology of the Mon R2 region

The Mon R2 region displays massive stars in apparently three successive stages of formation. The earliest stage is identified with the complex mm emission that suggests the formation of cold cores away from the IR sources [32]. The discrete, and more evolved, MYSOs in the COMICS image are separated by a ridge of mid-IR emission. At the maximum intensity along the mid-IR ridge, just on the inside close to the smaller of the two crosses, the diffuse nebulosity corresponds to the location of an extended HII region, the most advanced stage in this region, harbouring the near-IR source IRS1. Again the HII region does not have a discrete  $24.5\mu\text{m}$  counterpart.

The large-scale mid-IR shell structure has a near-IR counterpart [33]. The large cross in Fig. 1 corresponds to the centre of the CO J=3-2 “hole” as identified in [32]. Its morphology corresponds roughly to the extent of the HII region [34]. If we compare the mid-IR image with these maps, we can identify the  $24.5\mu\text{m}$  emission with the walls of the ionised region.

## 4. MYSO envelope structure from the SED and the $24.5\mu\text{m}$ intensity profile

The lack of asymmetries seen in the discrete and partially resolved MYSO envelopes warrants the use of simple spherical radiative transfer models. The envelopes can be described by powerlaws in density  $\rho = \rho_0 r^{-n}$ , where the power index  $n$  reveals the physics governing the structure. In this section we discuss in some detail two examples of simultaneously modelling the  $24.5\mu\text{m}$  emission and SED with aiming to extract the density power index from the observables. Simultaneous modelling seeks consistency between the spatial and spectral information. The size scale of the envelope depends strongly on  $L_{\text{bol}}$  determined from the far-IR and submm flux levels. The wavelength region  $< 10\mu\text{m}$  is ignored as various components other than the envelope may contribute. Two very different examples are presented: S140 IRS1 and M8E-IR. The case of the dominant MYSO in the Mon R2 region (IRS3) is nearly identical to S140 IRS1, and its modelling alongside other details of the modelling of our complete MYSO sample can be found in de Wit et al. 2008 (subm).

S140 IRS1 and M8E-IR are the brightest and dominant mid-IR sources in the respective regions. The SED continuum measurements from the literature are supplemented with ISO-SWS spectra that provide strong constraints for the total dust optical depth through the envelope by means of the  $9.7\mu\text{m}$  absorption feature. Data and models are presented in Fig. 2 and 3, models are fit to SED’s filled circles and ISO data.

S140 IRS1 is extended and clearly resolved. The length of the intensity profile errorbars cover the range of pixel values at each radial distance bin. Their small values indicate that IRS1 can be considered to be symmetric to first order. Various density distributions are able to fit the intensity profile as well. The simultaneous fit to the SED excludes however the shallower  $n = 0.5$  or the steeper  $n = 1.5$  powerlaws and  $n = 1.0$  is preferred. A steeper radial profile requires high optical depths and produces silicate absorption that is deeper than observed.

M8E-IR is compact and only marginally resolved at  $24.5\mu\text{m}$ . The spherical model that fits the intensity profile best has an  $n = 1.5$  powerlaw. It predicts however too little flux at long wavelengths for the envelope outer radii we initially assumed. In order to increase the (sub)mm flux levels without increasing the bolometric luminosity we make the envelope larger by adding cool material at the outer fringes. Depending on what the true (sub)mm flux is,  $n = 1.25$  to

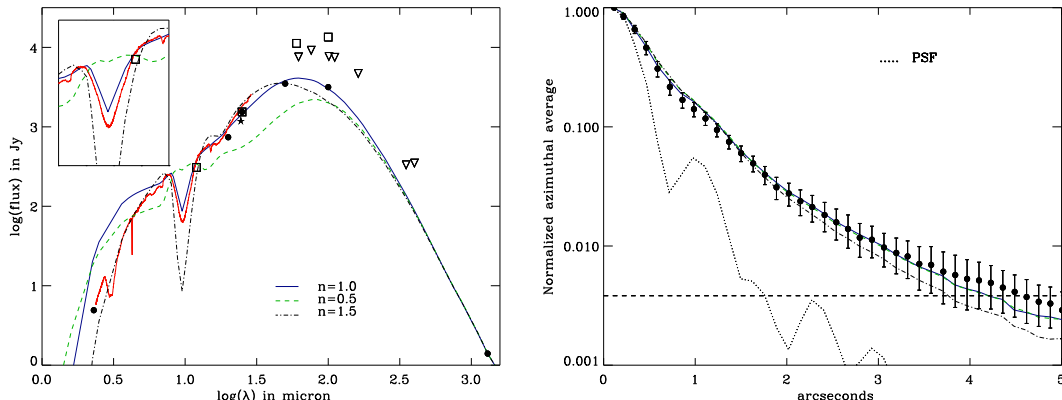


**Figure 2.** Observations and modelling of S140IRS1. *Left:* Asterisk: COMICS flux, filled circles: KAO 50 and 100  $\mu\text{m}$  [35], 1.3mm SEST [15]. Open symbols (not used in model fit): IRAS and submm data from [15, 36]. *Right:* 24.5  $\mu\text{m}$  intensity profile. The best simultaneous fitting model has a density profile with a  $n = 1.0$  powerlaw.

$n = 1.5$  are preferred with a relatively large outer radius of 1pc. The flux level of the ISO-SWS spectrum can however not be attained. The models are forced to fit the COMICS flux data point given the lack of unambiguous flux level at these wavelengths. We conclude that a spherical model is capable of reproducing both the 24.5  $\mu\text{m}$  profile and SED simultaneously for a dust density radial distribution of  $n = 1.25$  and an outer radius of 3000 times the inner radius. On scales of 1000-10 000 AU, the 350  $\mu\text{m}$  intensity profile is best represented by models with  $n = 1.75$  radial powerlaw density distributions [20].

In summary, for 60% of our MYSO sample spherical models are capable of satisfactorily reproducing the SED and intensity profile simultaneously. The fit includes a correct prediction for the depth of the silicate absorption profile at 9.7  $\mu\text{m}$ , the flux levels at 24.5  $\mu\text{m}$  and at (sub)mm wavelengths, and of course the 24.5  $\mu\text{m}$  intensity profile. The wavelength region that is least constrained by the data is the 100  $\mu\text{m}$  wavelength region (the peak of the SED), where in most cases the IRAS data points constitute the only flux measurement, however they have too coarse an angular resolution in our analysis.

Two objects (out of 10) can not be modelled with spherical models: AFGL 2591 and S255 IRS3. The  $L_{\text{bol}}$  and the size scale of the envelope are incompatible in these cases. M8E-IR actually poses similar problems regarding the mid-IR flux shortward of 25  $\mu\text{m}$ . In fact, there is excess mid-IR flux with respect to the spherical model that can only be accounted for if a higher  $L_{\text{bol}}$  is adopted, a solution denied by the intensity profile. It would suggest that mid-IR emission from these sources is not fully dominated by the envelope.

Noteworthy is that the MYSOs that have the poorest fits to spherical models (40%), are the ones represented by relatively steep radial density distributions. It is probably not a coincidence that all these sources have evidence for cavity wall emission or outflow activity along the line of sight. Their poor model fits probably reflect the inadequacy of spherical models.

The remaining six objects are well reproduced by spherical models and four of them have a preferred  $n = 1.0$  powerlaw. Two cases show even shallower density profiles. However in case of IRAS 20126 emission is most likely dominated by disk rather and/or outflow cavity emission [39]. Only little background information is available for the second flat source AFGL 437S. We can therefore conclude tentatively that when relatively steep spherical models fit MYSOs SEDs and intensity profiles, the source SED is probably not uniquely determined by envelope emission

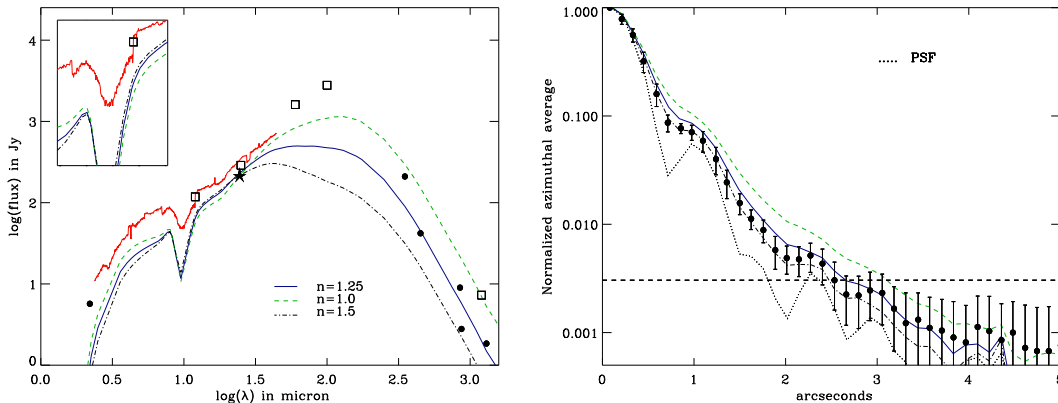


**Figure 3.** Observations and modelling of M8E-IR *Left:* Asterisk: COMICS flux, other data from [15, 20]. The level of (sub)mm continuum flux is uncertain, due to beam size effects. FWHM varies between  $9''$  ( $870 \mu\text{m}$ ) and  $30''$ . For reference the 1.2 mm data point by [37] with a FWHP of  $26''$  (open square). Short wavelength data by [38]. *Right:* The  $24.5 \mu\text{m}$  intensity profile. Best fitting model has a density powerlaw with  $n = 1.25$  index.

but partially by inhomogeneities in the envelope (cavity walls). Otherwise, for those MYSO where spherical models are capable of reproducing simultaneously the  $24.5 \mu\text{m}$  intensity profile and the SED, radial density profiles power index of  $n = 1.0$  on scales of 1000 AU are preferred.

### 5. Envelope emission at milli arcsecond scale resolution with VLTI/MIDI

Resolving the circumstellar environment of MYSO on scales of 0.05 arcseconds can be attained in interferometric mode with VLT and the MIDI instrument. MIDI operates at  $10 \mu\text{m}$  and delivers spectrally dispersed visibilities. Various components in the circumstellar environment of a MYSO may contribute to emission at wavelengths  $< 30 \mu\text{m}$ . Near-IR photons may originate either from the stellar surface, an inner dust truncation structure or from an accretion disk. They can easily scatter and escape through existing inhomogeneities in the spherical envelope [40] and still suffer extinction from any foreground molecular cloud material, e.g. [41]. Under favourable inclinations, mid-IR radiation from the surface of cavities sculpted by polar outflows can be seen. In this case, the mid-IR photons are emitted by warm dust particles that have a clear line-of-sight to the star, e.g. [39]. MIDI has the potential of revealing the geometry of the various interacting components involved in shaping a massive star (see also Linz et al. in these proceedings). We executed a MIDI program on the MYSO W33A aimed at resolving the  $10 \mu\text{m}$  emission, and determining which component of the MYSO environment dominates it.

The targeted MYSO, W33A, has a kinematic distance of 3.8 kpc and a luminosity as derived from IRAS fluxes of  $1 \times 10^5 L_{\odot}$  [42]. It has weak, compact, optically thick radio continuum emission [43, 44] and broad ( $\sim 100 \text{ km s}^{-1}$ ), single-peaked H I recombination emission lines [45] consistent with an ionised stellar wind origin. IR images from 2MASS and Spitzer’s GLIMPSE survey clearly show a large scale monopolar nebula emerging to the SE.

Fig. 4 presents the measured MIDI visibilities (with errorbars) and the SED. W33A shows a particularly deep silicate absorption feature. At the central wavelength of the feature no flux was recorded, and the actual depth is unknown. This is the reason why the visibility spectrum in Fig. 4 does not show any measurement between 9 and  $11 \mu\text{m}$ . The visibilities have a declining trend with wavelength. If we would represent the emission by a Gaussian emitting distribution then the FWHM size increases from 30 mas (115 AU) at  $8 \mu\text{m}$  to 60 mas (230 AU) at  $13 \mu\text{m}$ .

Modelling the  $10 \mu\text{m}$  emission is again performed with 1D DUSTY. Our basic aim is to probe

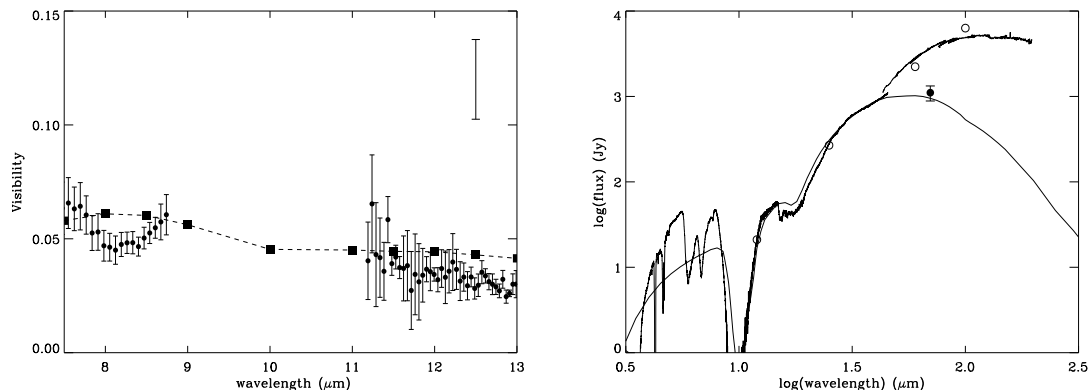


**Figure 4.** *Left:* MIDI visibilities of W33A (with errorbars). The dashed line is best fitting DUSTY model. *Right:* Simultaneous model fit to the SED. Shown are ISO spectra, and IRAS data. The data point with errorbar is from Spitzer MIPS.

whether the spatial and spectral information can be accounted for by envelope emission alone. Fitting 1D DUSTY models to the visibilities and SED of W33A shows that for nominal stellar parameters, the size scales of the emission region are too large and produce the wrong trend with wavelength. Relatively shallow radial density distributions with power indices between  $n = 0.5$  and  $n = 1.0$  reproduce better the observed dependency of size with wavelength. The deep silicate feature observed in the flux spectrum is better reproduced by dust models with warm Ossenkopf silicates that have an increased silicate over graphite ratio. For all models however the bolometric luminosity and  $T_{\text{eff}}$  of the central object need to be reduced. This reduction in  $L_{\text{bol}}$  is in fact in better agreement with  $70\,\mu\text{m}$  Spitzer photometry, as can be seen in Fig. 4. In summary, the reasonable fit with spherical models thus suggest that in case of W33A dominant component at  $10\,\mu\text{m}$  emission is the envelope.

The MIDI observations thus reveal that any circumstellar accretion disk structure should probably be smaller than the inner extent of the envelope, i.e.  $\sim 100\,\text{AU}$ . In addition, the reduction in  $T_{\text{eff}}$  would imply that the central star may be swollen. These results are consistent with the MIDI findings for M8E-IR as presented by Linz et al. (these proceedings). A bloated star would support the idea of induced swelling by high-mass accretion rates causing very large radii of the central object [46, 47].

## 6. Concluding remarks

High angular resolution mid-IR observations are starting to give a clear and detailed view of how the circumstellar material of a MYSO is organised. In this contribution we have presented an analysis of circumstellar emission of MYSOs in the mid-IR at two different wavelengths ( $24.5\,\mu\text{m}$  and  $10\,\mu\text{m}$ ) and two different resolutions ( $0.6''$  and  $0.05''$ ). We have found that when the emission at these wavelengths is dominated by dust emission from the envelope the radial density profiles can be described by a powerlaw of the form  $\rho = \rho_0 r^{-n}$  with a power index of approximately  $n = 1.0$ . Steep powerlaws  $n \geq 1.5$  are excluded as they require high optical depth denied by the silicate absorption profile. Steep powerlaws are found but only in those cases where there is evidence for a contribution by the outflow cavity to the mid-IR emission. We note that our results for the radial density distribution does not negate the findings of previous studies conducted in the (sub)mm wavelength region. For example [20] claim a value of  $1.8 \pm 0.4$  from analysis for  $350\,\mu\text{m}$  intensity profiles. However our results seem to be more in line with lower values found by [19]. The powerlaw dependence of density with radius is predicted to have a

powerindex of  $n = 1.0$  when the envelope is supported by turbulence [48], although on the scales probed with MIDI rotational flattening may start to play a significant role.

## References

- [1] McKee C F and Tan J C 2003 *ApJ* **585** 850
- [2] Bonnell I A, Bate M R, Clarke C J and Pringle J E 1997 *MNRAS* **285** 201
- [3] Krumholz M R and Tan J C 2007 *ApJ* **654** 304
- [4] Motte F, Bontemps S, Schilke P, Schneider N, Menten K M and Brogière D 2007 *A&A* **476** 1243
- [5] Alves J, Lombardi M and Lada C J 2007 *A&A* **462** L17
- [6] Baines D, Oudmaijer R D, Porter J M and Pozzo M 2006 *MNRAS* **367** 737
- [7] Edgar R and Clarke C 2004 *MNRAS* **349** 678
- [8] Krumholz M R 2006 *ApJ* **641** L45
- [9] Zinnecker H and Yorke H W 2007 *ARA&A* **45** 481
- [10] McKee C F and Ostriker E C 2007 *ARA&A* **45** 565
- [11] Beuther H and Shepherd D 2005 *Cores to Clusters: Star Formation with Next Generation Telescopes* ed Kumar M S N, Tafalla M and Caselli P pp 105–119
- [12] Chini R, Kruegel E and Kreysa E 1986 *A&A* **167** 315
- [13] Churchwell E, Wolfire M G and Wood D O S 1990 *ApJ* **354** 247
- [14] Hoare M G, Roche P F and Glencross W M 1991 *MNRAS* **251** 584
- [15] Guertler J, Henning T, Kruegel E and Chini R 1991 *A&A* **252** 801
- [16] Wolfire M G and Churchwell E 1994 *ApJ* **427** 889
- [17] Faison M, Churchwell E, Hofner P, Hackwell J, Lynch D K and Russell R W 1998 *ApJ* **500** 280
- [18] Hatchell J, Fuller G A, Millar T J, Thompson M A and Macdonald G H 2000 *A&A* **357** 637
- [19] van der Tak F F S, van Dishoeck E F, Evans II N J and Blake G A 2000 *ApJ* **537** 283
- [20] Mueller K E, Shirley Y L, Evans II N J and Jacobson H R 2002 *ApJS* **143** 469
- [21] Beuther H, Schilke P, Menten K M, Motte F, Sridharan T K and Wyrowski F 2002 *ApJ* **566** 945
- [22] Kataza H, Okamoto Y, Takubo S, Onaka T, Sako S, Nakamura K, Miyata T and Yamashita T 2000 *Proc. SPIE Vol. 4008* vol 4008 ed Iye M and Moorwood A F p 1144
- [23] de Wit W J, Hoare M G, Oudmaijer R D and Mottram J C 2007 *ApJ* **671** L169
- [24] Ivezić Z and Elitzur M 1997 *MNRAS* **287** 799
- [25] Crampton D and Fisher W A 1974 *Spectroscopic observations of stars in HII regions* (Victoria : National Research Council of Canada, Radio and Electrical Engineering Division, Astrophysics Branch, 1974.)
- [26] Beichman C A, Becklin E E and Wynn-Williams C G 1979 *ApJ* **232** L47
- [27] Hoare M G 2006 *ApJ* **649** 856
- [28] Jiang Z, Tamura M, Hoare M G, Yao Y, Ishii M, Fang M and Yang J 2008 *ApJ* **673** L175
- [29] Preibisch T, Balega Y Y, Schertl D, Smith M D and Weigelt G 2001 *A&A* **378** 539
- [30] Evans II N J, Mundy L G, Kutner M L and Depoy D L 1989 *ApJ* **346** 212
- [31] Minchin N R, Ward-Thompson D and White G J 1995 *A&A* **298** 894
- [32] Giannakopoulou J, Mitchell G F, Hasegawa T I, Matthews H E and Maillard J P 1997 *ApJ* **487** 346
- [33] Howard E M, Pipher J L and Forrest W J 1994 *ApJ* **425** 707
- [34] Massi M, Felli M and Simon M 1985 *A&A* **152** 387
- [35] Lester D F, Harvey P M, Joy M and Ellis Jr H B 1986 *ApJ* **309** 80
- [36] Thronson Jr H A, Lada C J, Smith H A, Glaccum W, Harper D A, Schwartz P R and Knowles S H 1983 *ApJ* **271** 625
- [37] Beltrán M T, Brand J, Cesaroni R, Fontani F, Pezzuto S, Testi L and Molinari S 2006 *A&A* **447** 221
- [38] Simon M, Peterson D M, Longmore A J, Storey J W V and Tokunaga A T 1985 *ApJ* **298** 328
- [39] De Buizer J M 2007 *ApJ* **654** L147–L150
- [40] Henning T, Schreyer K, Launhardt R and Burkert A 2000 *A&A* **353** 211
- [41] De Buizer J M, Osorio M and Calvet N 2005 *ApJ* **635** 452
- [42] Faúndez S, Bronfman L, Garay G, Chini R, Nyman L Å and May J 2004 *A&A* **426** 97
- [43] Rengarajan T N and Ho P T P 1996 *ApJ* **465** 363
- [44] van der Tak F F S and Menten K M 2005 *A&A* **437** 947
- [45] Bunn J C, Hoare M G and Drew J E 1995 *MNRAS* **272** 346
- [46] Hoare M G and Franco J 2007 *ArXiv e-prints (Preprint 0711.4912)*
- [47] Hosokawa T and Omukai K 2008 *Evolution of Massive Protostars with High Accretion Rates (Astronomical Society of the Pacific Conference Series* vol 387) ed Beuther H, Linz H and Henning T p 255
- [48] Lizano S and Shu F H 1989 *ApJ* **342** 834